International Journal of Applied Earth Observation and Geoinformation 121 (2023) 103378

Contents lists available at ScienceDirect

International Journal of Applied Earth Observation and Geoinformation

journal homepage: www.elsevier.com/locate/jag

# Agricultural drought conditions over mainland Southeast Asia: Spatiotemporal characteristics revealed from MODIS-based vegetation time-series

Tuyen V. Ha [a,b,c,*], Soner Uereyen [a], Claudia Kuenzer [a,b]

[a] German Remote Sensing Data Center, German Aerospace Center, Oberpfaffenhofen, 82234 Wessling, Germany
[b] University of Wuerzburg, Institute of Geography and Geology, Am Hubland, 97047 Wuerzburg, Germany
[c] Faculty of Resource Management, Thai Nguyen University of Agriculture and Forestry, Thai Nguyen 24000, Vietnam

ARTICLE INFO

*Keywords:*
Drought characteristics
Drought trend
Agricultural drought
Remote sensing
VCI

ABSTRACT

Drought is a reoccurring slow-onset hazard event and has a tremendous impact on agricultural production and ecosystem health. Mainland Southeast Asia is a major rainfed crop-producing area of the world, and this region is increasingly vulnerable to drought hazards. However, the monitoring and characterization of agricultural and vegetative droughts in this region remains understudied. This paper presented the first comprehensive analysis of spatiotemporal characteristics and trends of agricultural and vegetative droughts across the region using the Vegetation Condition Index (VCI) based on the reconstructed MODIS-based vegetation time-series data between 2000 and 2021. This study also developed an approach for identifying severe drought years using annual extreme pixels. Results showed that vegetation-based drought characteristics and trends varied in space and time across the region. Central Myanmar suffered from the most frequent droughts (nearly 60%), but prolonged events were less common. By contrast, the Lower Mekong area suffered from frequent and prolonged drought conditions. Most of the recent severe droughts were observed in Cambodia, and this area is characterized by a drying trend. Regionally, the severe drought years were detected in 2000, 2004, 2005, 2010, 2016, 2019, and 2020, and they were commonly found in Central Myanmar, Thailand, and Cambodia. The analysis of drought years indicated that the temporal change pattern of drought has shifted from the northern regions (e.g., Central Myanmar) in 2010 to the Lower Mekong region in recent years. The findings of this study provide valuable information for drought early warning management and agricultural planning across mainland Southeast Asia.

## 1. Introduction

Droughts are considered the costliest disaster among natural catastrophes, with widespread damage to agricultural production (Ha et al., 2022), ecosystem (Lingfeng et al., 2022), and the economy (Ding et al., 2011). Drought occurs in most climatic zones, and its impact on agriculture is the first and greatest, but it is the least understood of all natural disasters (Muthumanickam et al., 2011). Although there have been various definitions of drought over the past decades given differences in specific disciplines and sectors, drought is generally defined as a lack of rainfall over an extended period of time, resulting in a shortage of water supplies for the environment, economy, and society (Wilhite and Glantz, 1985). According to Dracup et al. (1980), drought is mainly classified as meteorological, agricultural, socioeconomic, and hydrological droughts. The lack of precipitation below the long-term average (e.g., 30 years), also known as meteorological drought, can be considered the origins of all types of drought (Ha et al., 2022), while agricultural drought refers to a lack of soil moisture content that causes vegetative stress and/or crop failure (Mishra and Singh, 2010). Despite its different types, a drought event is identified by some common characteristics (e.g., frequency and duration). These traits likely have different impacts on agriculture and the ecosystem. For example, short severe droughts can damage crops in the seedling stage (Unganai and Kogan, 1998), whereas prolonged low-intensity events can have disastrous consequences for the local environment and water resources (Lingfeng et al., 2022).

Historically, drought monitoring and assessment have been primarily undertaken using in-situ climatic indices such as the Standardized

* Corresponding author.
*E-mail address:* tuyenmassey@gmail.com (T.V. Ha).

https://doi.org/10.1016/j.jag.2023.103378
Received 6 February 2023; Received in revised form 27 April 2023; Accepted 26 May 2023
Available online 1 June 2023

Precipitation Index (McKee et al., 1993) and Standardized Precipitation Evapotranspiration Index (Vicente-Serrano et al., 2010). Although these station-based indices are considered the most reliable methods for monitoring drought (Wilhite and Glantz, 1985), they are costly and usually unable to provide large-area and near-real-time drought information (Jiao et al., 2021), especially in developing countries with sparse-data networks. Also, climate-based drought indices can not directly measure the impact of drought on vegetation health or productivity (Gebrehiwot et al., 2011). By contrast, earth observation time-series data have proven to be a powerful tool that provides timely drought information with spatial details. For instance, remote sensing vegetation-based drought indices offer direct insights into the impact of drought on vegetation and ecosystem health (Du et al., 2013; Gebrehiwot et al., 2011). With the growing accessibility of openly available remote sensing data, frequent monitoring and characterization of global and regional droughts over several decades have become possible, especially with the arrival of the Moderate Resolution Image Spectroradiometer (MODIS) and the Advanced Very High Resolution Radiometer (AVHRR).

Over the past decades, many vegetation-based remote sensing indices have been established and applied for drought monitoring, such as the Vegetation Condition Index (VCI) (Liu and Kogan, 1996), the Normalized Difference Vegetation Index (NDVI) (Tarpley et al., 1984), and the Soil-adjusted Vegetation Index (SAVI) (Huete, 1988). One of the most widely used indices for drought-related monitoring is the NDVI (Jiao et al., 2021) because the greenness of the land surface reflects well plant health and density. However, the use of NDVI might be limited due to its responses to atmospheric effects and soil reflection. Several other vegetation-based indices were subsequently proposed to overcome these drawbacks. For example, the SAVI was established to remove the soil constraints, while the VCI was proposed to enhance both atmospheric and soil components (Liu and Kogan, 1996). Among them, the VCI has been widely adopted as a drought indicator, and the World Meteorological Organization (WMO) suggested the VCI for global and local drought-related monitoring (Svoboda and Fuchs, 2016). The VCI has successfully used to detect agricultural and/or vegetative drought events worldwide, for example in Africa (Gebrehiwot et al., 2011; Unganai and Kogan, 1998; Winkler et al., 2017), in the United States (Kogan, 1995b), in China (Li et al., 2013; Liang et al., 2017; Qian et al., 2016; Yan et al., 2016), and in Iran (Bajgiran et al., 2008).

Mainland Southeast Asia (MSEA) is a major global rainfed crop-growing region. As a result of amplified global warming and human activities, this region becomes more susceptible to drought hazards (Amnuaylojaroen and Chanvichit, 2019; Zhang et al., 2021). In recent years, annual agricultural losses due to drought-related hazards have estimated at approximately US $19 billion (UNESCAP, 2019). Despite the increasing drought risks, the region has received limited attention in drought studies using remote sensing time-series in the past decades (Ha et al., 2022). For instance, Son et al. (2012) used MODIS-based vegetation-temperature data to monitor drought during the dry seasons (2002–2010) in the Lower Mekong region, while Xie and Fan (2021) assessed different reconstruction methods of MODIS Land Surface Temperature (LST) and vegetation data for drought detection. Other studies focused on the drought impact of rice crops (Son and Thanh, 2022; Venkatappa et al., 2021) and landcover/vegetation changes (Le et al., 2020; Zhang et al., 2014). The consistent observations of regional drought behaviors are of great importance, given differences in trends and spatiotemporal characteristics. Understanding these characteristics is crucial for supporting drought risk management, early warning, and agricultural planning to ensure regional food security as well as environmental sustainability. However, there have been no comprehensive studies of spatiotemporal drought characteristics and trends over the region using long-term remote sensing time-series observations (Ha et al., 2022). In this study, we present the first comprehensive analysis of spatiotemporal drought characteristics and trends over the entire MSEA region from 2000 to 2021.

The main objective of this work is to monitor and characterize the space–time trend and variability of agricultural and vegetative drought conditions over the MSEA using the VCI method and monthly MODIS-based vegetation time-series from 2000 to 2021. The specific objectives are to (1) identify severe drought years, (2) describe spatiotemporal characteristics of drought (e.g., drought events, years of latest drought, drought duration, and frequency, (3) investigate the time-series evolution of the drought conditions across cropland vegetations, (4) explore the trend in drought conditions, and (5) evaluate the results of VCI with climatic factors. The findings of this study are of great value for the current and future efforts towards drought risk management and agricultural planning in the MSEA region.

## 2. Study area and materials

### 2.1. Study region

The study area covers five different countries in the MSEA region with a total area of nearly 2 million km$^2$ (Fig. 1). This region is home to approximately 240 million people, and nearly 60% of its population relies on agricultural activities (Li et al., 2022). Rice becomes a staple food and is primarily cultivated in the Red River Delta, the Lower Mekong areas, and southern Myanmar. Overall, there are five main land cover types, including cropland, grassland, forest, shrubland, and others (e.g., water surface, bare-land, and residential areas) in the region. Cropland and forest account for the largest areas with 38% and 41.5%, respectively. Rainfed-based croplands account for the largest share, with nearly 85% (ESA, 2017).

The red squares in Fig. 1 highlight four exemplified provinces in the major crop-growing regions with different cropping practices. Rainfed agriculture is largely practiced in Cambodia, Myanmar, and Thailand, whereas Vietnamese rice fields are highly irrigated (Kuenzer and Knauer, 2013). For example, triple and double rice crops are commonly grown in Can Tho and Vinh Phuc provinces of the Lower Vietnamese Mekong and Red River areas, respectively whereas single-crop rainfed rice is largely cultivated in the Cambodian province of Kompong Chnang. By contrast, the agricultural system in Central Myanmar primarily relies on rainfed pulses and sesame (Herridge et al., 2019).

The weather in the region varies across landscapes and seasons and falls within the tropical monsoon climate zone. For example, the line and bar plots from Fig. 1 show the variations of monthly temperature and precipitation in four major crop-growing areas over the 21-year period, respectively. Generally, higher temperatures and lower precipitation are observed in Central Myanmar, while the Lower Mekong and Red River areas have the opposite patterns. The dry season has the least precipitation and highest temperature, for example in Central Myanmar with less than 10 mm/month and exceeding 35 °C. The monsoon climate characteristics facilitate two main growing seasons in the region: dry (winter) roughly from Nomvember to May and wet (summer) from June to December, and rice crops are largely grown during both seasons.

### 2.2. Data source

#### 2.2.1. MODIS NDVI time-series

MODIS dataset is a primary source of input for global and local ecosystem monitoring and assessment, including drought. Here, the NDVI observations were extracted from the latest version (6.1) MOD13A2 (Terra) and MYD13A2 (Aqua) 16-day products. The NDVI measures the vegetation greenness, and its calculation is based on the normalized difference between two bands: red and near infrared reflectance (Didan et al., 2015). Given the frequent cloud cover over the tropical region (Leinenkugel et al., 2013), this study utilized both sensors to maximize cloud-free pixels. In recognition of the analysis-ready data, the U.S. Geological Survey (USGS) performed various measurement uncertainty corrections (e.g., geometric and atmospheric corrections) and produced the NDVI products (Didan, 2021). Each NDVI 16-

day composite image selects the best available daily NDVI pixels from the acquisition of 16 days. This dataset is identified in a Sinusoidal grid system and then converted into a geographic coordinate system and accessed through the Google Earth Engine (GEE) cloud platform. A total number of 951 images are available over the MSEA region between 2000 and 2021 at 1 km pixel resolution.

### 2.2.2. Land cover data

Climate Change Initiative (CCI) program of the European Space Angency (ESA) offers global landcover maps from 1992 to the present. This product is annually updated and consists of 37 landcover classes at 300 m spatial resolution (ESA, 2017). The GlobCover unsupervised and supervised classification methods are combined to generate the consistent ESA CCI land cover products from multiple satellites (e.g., PROBA-V and SPOT). In this study, the product 2016 was undertaken to investigate different vegetation types across the region. This dataset was created from the PROBA-V satellite, and each pixel was enhanced with multi-year observations to minimize the classification errors (ESA, 2017). Given the primary land covers of the MSEA region, we reclassified the 37 classes into five main land cover types: cropland, forest, grassland, shrubland, and others. This dataset was subsequently aggregated to 1 km spatial resolution using the nearest neighbor technique to match the MODIS NDVI product.

### 2.2.3. Precipitation and temperature data

Temperature and rainfall were obtained from MODIS LST and the Climate Hazards Group Infrared Precipitation with Station (CHIRPS) products, respectively, to evaluate the results of the drought observations. The monthly LST was retrieved from the daytime MOD11A2 - product (version 6.1) from 2000 to 2021 using the mean value

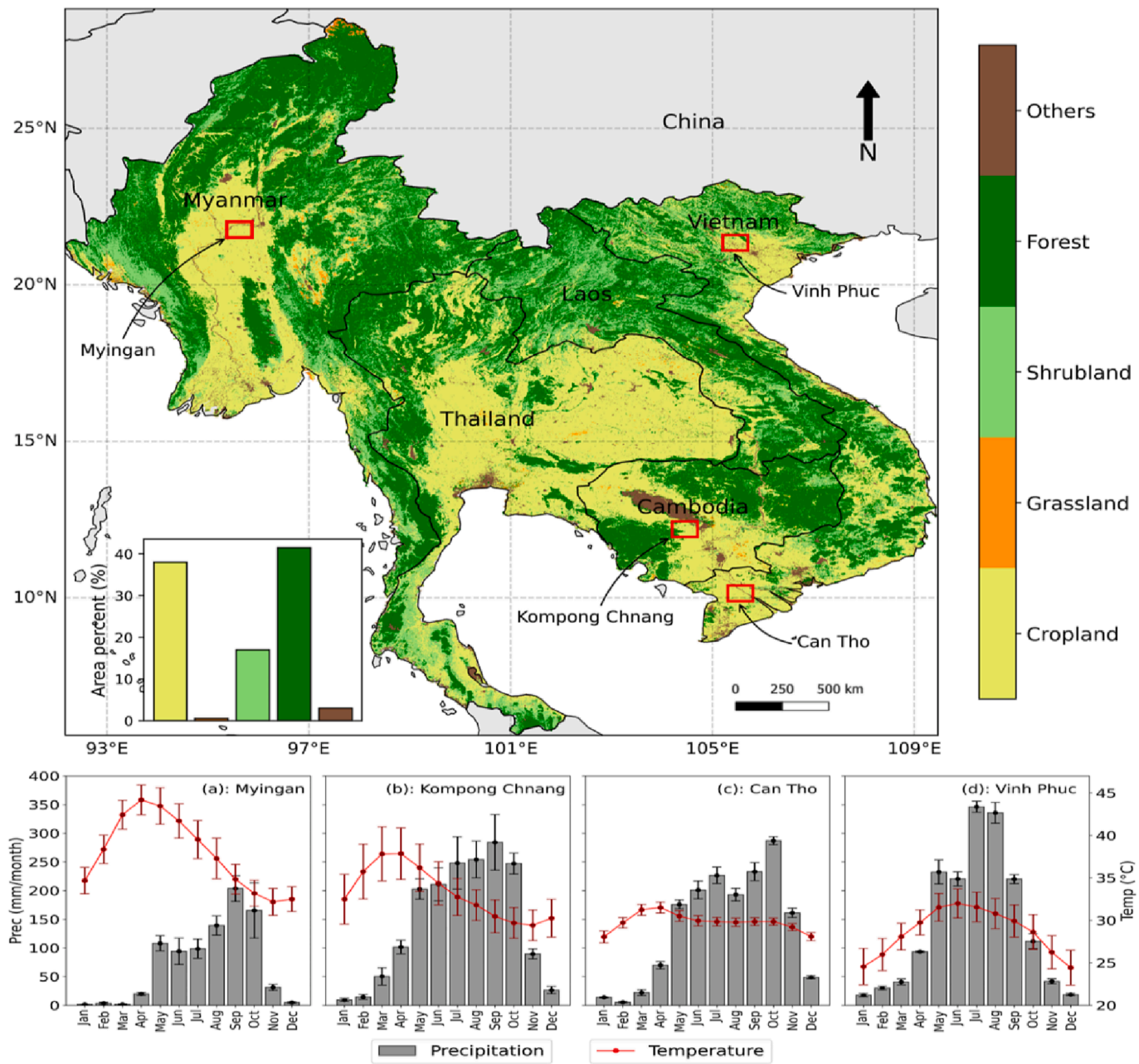


**Fig 1.** Map of the MSEA countries with five land cover types and their percentages (sub-bar plot). The bar and line plots display the seasonality of mean rainfall and temperature, respectively in (a) Myingan (Myanmar), (b) Kompong Chnang (Cambodia), and (c) Can Tho and (d) Vinh Phuc (Vietnam) from 2000 to 2021. Vertical lines represent ± standard deviation. The map and its administrative names are extracted from GADM (https://gadm.org/).

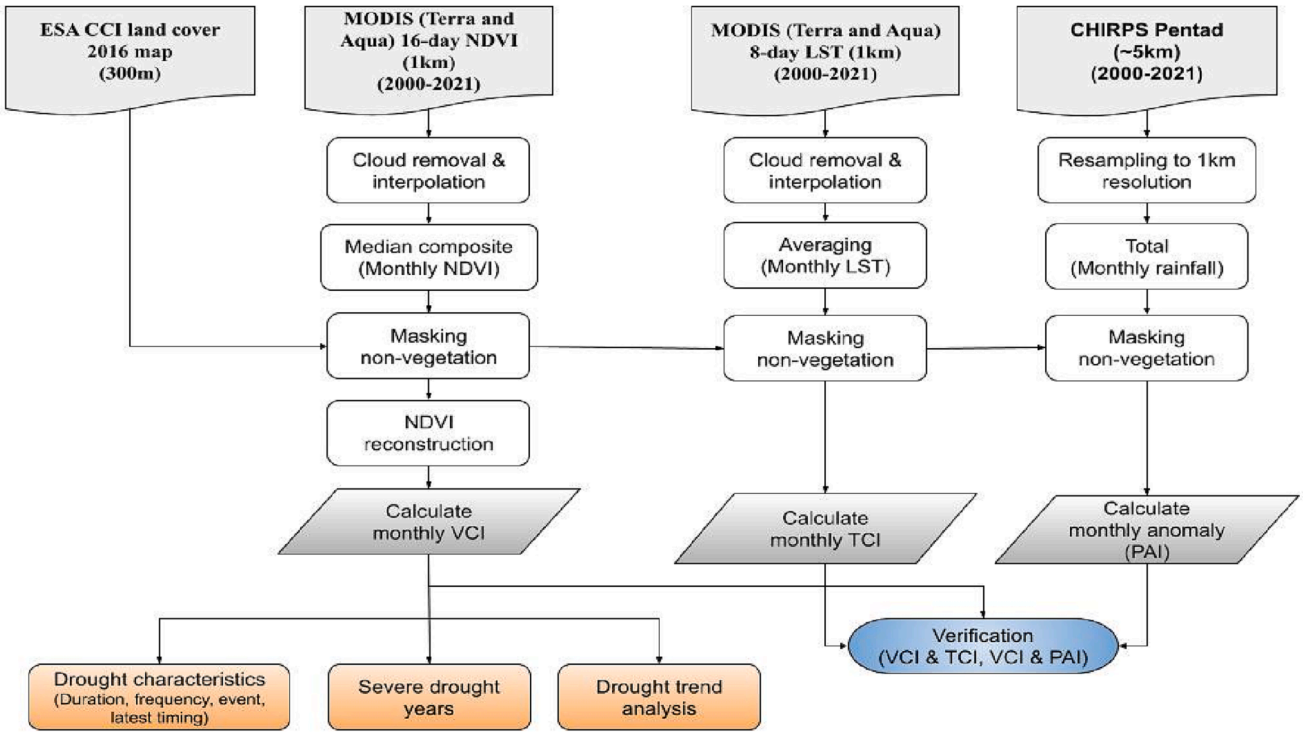


**Fig. 2.** An overview of drought monitoring and characterization from data preprocessing to derived products and verification.

composite. Here, cloud-contaminated LST values were eliminated to include only clear-sky observations whereas missing values were interpolated using the nearest neighbor value. In addition, we used the long-term CHIRPS pentad product, which provides quasi-global coverage (~5km spatial resolution) from 1981 to the present. This dataset is produced using the infrared cold cloud duration observations of multiple satellites (e.g., TRMM and NOAA GridSat) and subsequently enhanced with station-based measurements (Funk et al., 2015). In the MSEA region the CHIRPS product outperformed other satellite-based precipitation products (Dandridge et al., 2019). The CHIRPS data was also resampled to higher spatial resolution (1 km) using the bilinear method.

## 3. Method

This section presents the workflow of spatiotemporal monitoring and characterization of agricultural and vegetative drought conditions in the MSEA region from 2000 to 2021. To obtain the consistent and continuous observations of drought, the high-quality MODIS NDVI time-series were reconstructed and utilized to derive the monthly VCI values. The auxiliary datasets are pre-processed to suit the spatio-temporal resolutions of the MODIS NDVI measurements. Subsequently, drought characteristics and trends are derived based on the VCI time-series, whereas a robust approach for identifying severe drought years was proposed. Ultimately, the LST and precipitation were used to verify the results of the VCI-based drought conditions. An overview of the implemented workflow is presented in Fig. 2.

### 3.1. Reconstruction of MODIS NDVI time-series

In the MSEA region, persistent clouds and shadows in the optical remote sensing data impede the continuous derivation of accurate drought observations. Reconstruction of time-series measurements is therefore essential to minimize noise, produce gap-free pixels, and enhance drought detection. For this study, the NDVI observations are interpolated and composited in a monthly window and subsequently reconstructed using the Savitzky–Golay (SG) filter method.

A linear interpolation is applied for the NDVI time-series observations from 2000 to 2021 (Chen et al., 2004). Subsequently, the monthly NDVI data were composited in a monthly window using the median value composite (MVC) method, which takes the median value of the NDVI time series in a given month as the composited value. This method proved to be more stable and robust to outliers (Ruefenacht, 2016). A total number of 263 monthly NDVI reconstructed images are available over the MSEA region from 2000 to 2021. Due to the effects of persistent clouds and interpolation technique, the SG method is undertaken to produce noise-free monthly NDVI time-series. This method was widely accepted because it preserves the temporal curve of the NDVI measurements and produces better drought indices. The concept of the SG filter is to fit a polynomial least-squares equation in a local moving window to enhance vegetation observations (Chen et al., 2004). Two key parameters are required for this method: the polynomial orders and window size, and this study used the values 2 and 5, respectively.

### 3.2. Vegetation condition index (VCI)

The NDVI was widely accepted to detect drought conditions and vegetation stress, but the interpretive issues might arise in heterogeneous vegetative areas (Kogan, 1990). This means vegetation health is likely attributed to environmental and atmospheric variations. In comparable areas, for example, higher NDVI values were found in areas with excessive resources (e.g., more favorable climate and soil) than in areas with underprivileged conditions (Kogan, 1990). This disparity is mainly due to weather and ecosystem components. Due to poor signal of climatic elements, the weather-induced vegetation changes are more challenging to identify than that of ecological components. Thus, the climatic components should be removed from the ecosystem factors when we used the NDVI for monitoring weather-related impacts in terrestrial vegetation (Kogan, 1990).

Developed by Kogan (1990), the VCI was designed to enhance the weather-related components in the NDVI value. Here, the linear transformation is applied for scaling the vegetation (NDVI) values from zero (minimum NDVI) to 100 (maximum NDVI) at each pixel across time

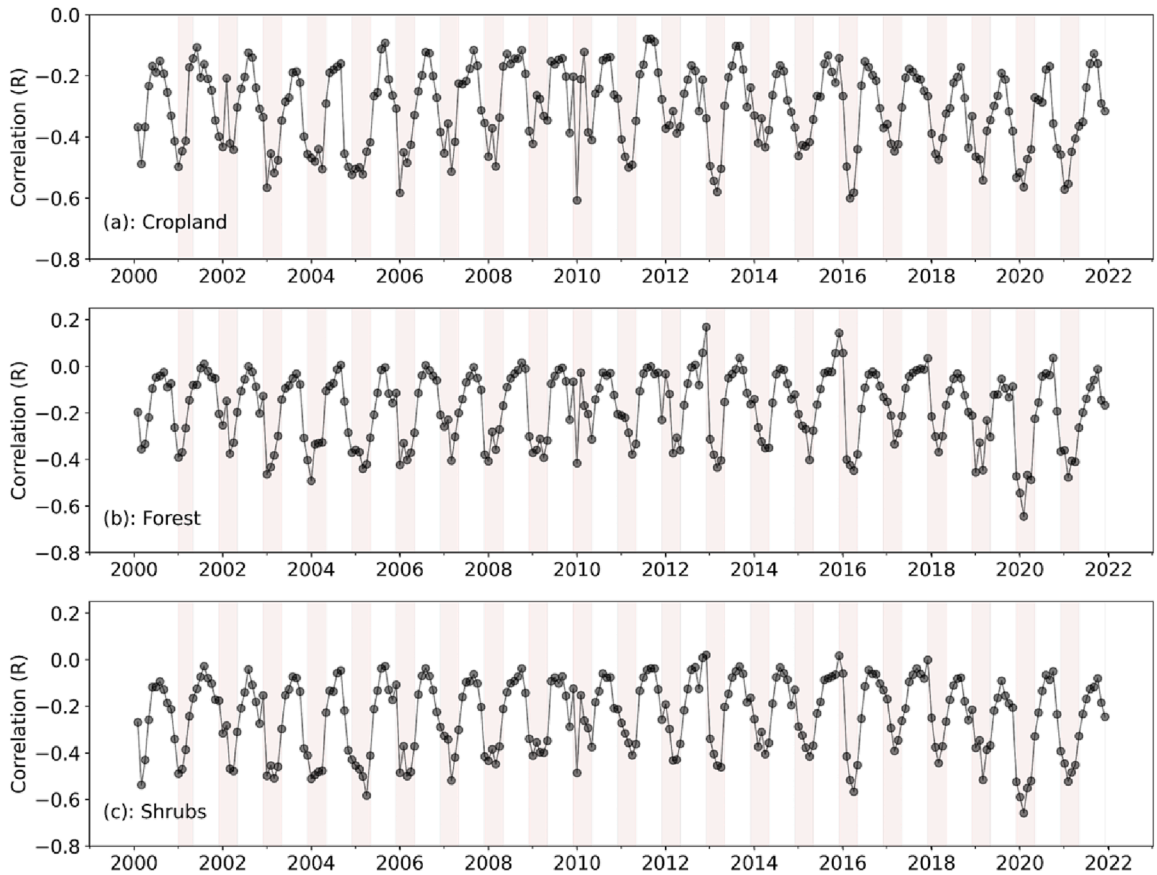


**Fig. 3.** Monthly correlation between the VCI and TCI for cropland (a), forest (b), and shrubland (c) over the MSEA region from 2000 to 2021. The shaded color bar indicates dry months from December to May.

period. The VCI is computed by the following expression (Eq. (1)):

$$VCI_i = 100^* \frac{NDVI_i - NDVI_{min}}{NDVI_{max} - NDVI_{min}} \tag{1}$$

While $NDVI_i$ is the monthly NDVI, $NDVI_{max}$ and $NDVI_{min}$ are the highest and lowest NDVI values, respectively, computed at each pixel and monthly interval (12 months) using the examined NDVI record (2000–2021). The VCI measurements are identified in percentages ranging between zero and 100, reflecting vegetation health conditions from very poor (drought) to healthy (non-drought). Following Kogan (1995a) and (Dutta et al., 2015), we classified the VCI into five levels of drought severity. We defined values from 50 to 100% as non-drought, and the value from 30% to 50% represents a mild drought. Moderate drought ranges from 20% to 30%, whereas the VCI below 10% and 20% shows extreme and severe droughts, respectively.

### 3.3. Identification of severe drought years and characteristics

Drought characteristics and severe drought years were detected using the monthly VCI-based drought observations between 2000 and 2021. A severe drought year can cause widespread and long-lasting impacts on crops, livestock, and ecosystems, resulting in food insecurity, economic loss, and environment degradation. Most of the previous studies defined the VCI-based extreme and severe drought conditions less than 20% (Gebrehiwot et al., 2011; Kogan, 1995a; Shahabfar et al., 2012). In this study, we tested different threshold values (from 5% to 20%) and evaluated their performance with the in-situ drought reported years in the MSEA region. We found that the 10% threshold value aligned the most with the reported drought years. Therefore, a severe drought year is defined as the annual percentage of extreme pixels (VCI $\leq$ 10%) exceeding the long-term (21 years) average (Eq. (2)), while we also considered the extreme VCI severity over the same period (Eq. (3)).

$$P_i = \frac{\sum_1^j \left(\frac{VCI_{i,j}}{N}\right) 100\%}{M_i} \quad (VCI \leq 10\%) \tag{2}$$

Where $P_i$ and $M_i$ are the percentage of extreme pixels and number of months at year $i$, respectively. The $VCI_{i,j}$ is the total VCI value at month $j$ in year $i$ whereas $N$ is the total number of valid pixels (excluded NANs valued) across the region.

$$S_i = \frac{\sum_1^j (A_{i,j})}{M_i} \quad (VCI \leq 10\%) \tag{3}$$

Where $S_i$ and $M_i$ are annual average VCI values and number of months at year $i$, respectively. The $A_{i,j}$ is the mean VCI value at month $j$ in year $i$ across the region where the VCI pixels ($\leq$10%) are considered.

In addition, we investigated four main characteristics of drought in each grid cell: number of drought events, latest drought year, drought frequency, and drought duration. To identify these characteristics, we defined a drought event as continuous VCI value less than 50%. This threshold was chosen because prolonged mild to moderate drought conditions might cause a considerable damage to crop production and the ecosystem (Guo et al., 2018). Also, this threshold can be helpful for developing and implementing a drought early warning system. In this study, the number of drought events reflects the drought conditions with a continuous consecutive VCI below the threshold value for at least three months, while the drought duration is the average length of drought from 2000 to 2021. The drought year represents the latest years with the maximum consecutive drought months, and the drought frequency is the occurance drought events over the selected study period.

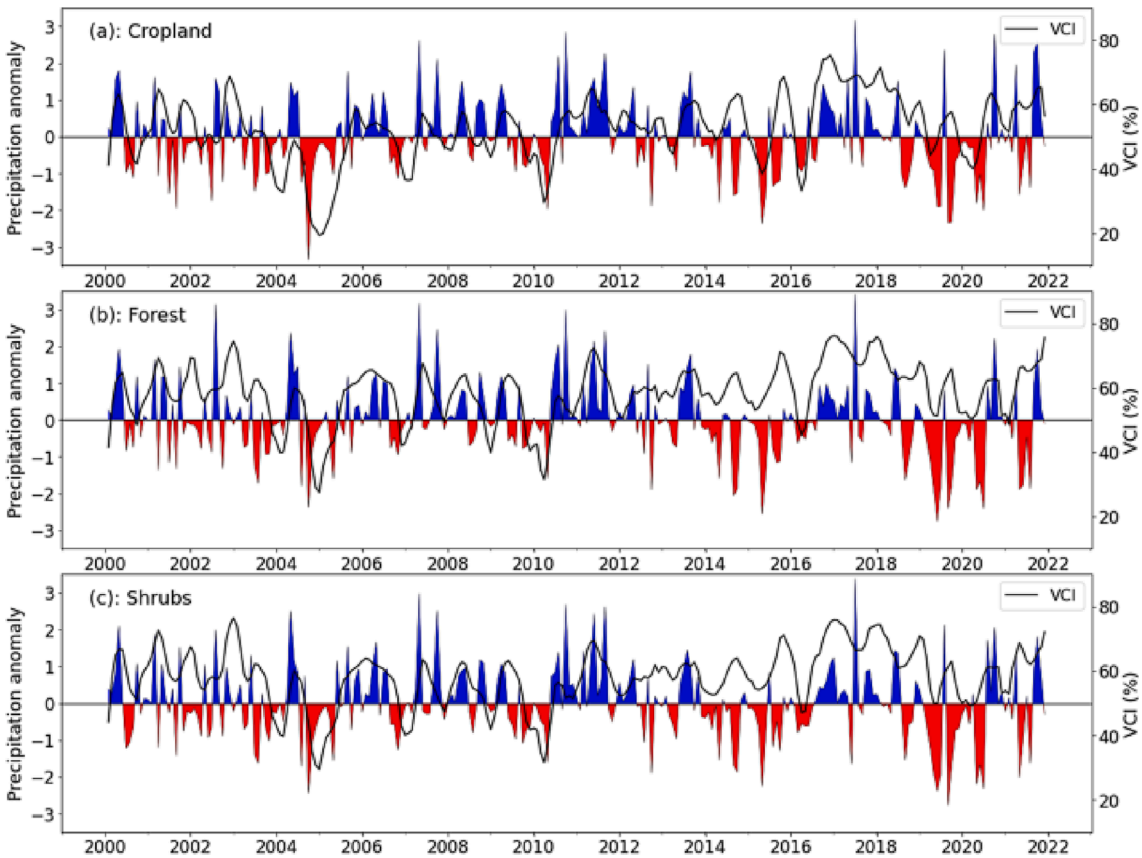


**Fig. 4.** Temporal variations of VCI and precipitation anomaly for cropland (a), forest (b), and shrubland (c) over the MSEA region from 2000 to 2021. Blue and red colors represent a precipitation anomaly above or below the long-term average.

### 3.4. Time-series analysis

Parametric and non-parametric methods were commonly used to perform trends of land surface variables from remote sensing time-series measurements (Mao et al., 2012). This study used non-parametric methods because they are robust to autocorrelated and non-normally distributed data (Fan et al., 2017). Here, we employed the Mann-Kendall (MK) statistical test together with Sen's slope method for detecting the significance of interannual drought trends over the two main growing seasons, summer (rainy) and winter (dry), from 2000 to 2021. The MK test and Sen's slope were developed by Mann and Kendall (Guo et al., 2018) and became a widely used non-parametric methods due to their robustness to non-normality and missing values (Fan et al., 2017). The MK significance test identifies the trend's power and direction, whereas the Sen's slope measures the slope gradient (Sen, 1968). This study detected the drought trends at a significant level of $\alpha \leq 0.05$, where a positive (negative) slope indicates a significant increase (decrease) in drought conditions.

### 3.5. Verification of the VCI-based drought conditions

In-situ climatic factors (e.g., precipitation and temperature) are considered the most reliable for detecting drought conditions. However, collecting such data over large areas is very challenging due to sparse in-situ measurement networks, particularly over the MSEA region. Here, the monthly CHIRPS precipitation and MODIS-based LST datasets, therefore, were performed to verify the VCI results. The LST and precipitation observations were transformed to the temperature and precipitation standardized anomaly to avoid the effect of seasonality as expressed in Eq. (4), respectively.

$$SAI_{i,j} = \frac{CV_{i,j} - \overline{CV}_{i,j}}{\sigma_j} \tag{4}$$

While $SAI_{i,j}$ is the temperature and precipitation standardized anomaly for month $j$ and year $i$ over the selected study period, the $CV_{i,j}$ means the temperature and precipitation values in month $j$ and year $i$. The $\overline{CV}_{i,j}$ and $\sigma_j$ represents the average and standard deviation values of the temperature and precipitation at month $j$.

The Pearson correlation coefficient (R) and visual comparison were undertaken to examine the region-wide agreement between the VCI and the temperature and precipitation, respectively. We computed monthly R values between the VCI and temperature data for different vegetation classes across the region at a significance level ($\alpha \leq 0.05$). The R value runs from −1 to 1, with a higher absolute R value indicating a stronger correlation between the VCI and temperature. Finally, the VCI results were compared with precipitation for different land covers from 2000 to 2021.

## 4. Results and discussion

### 4.1. Cross-verification of the VCI-based drought condition with precipitation and temperature

Vegetation dynamics are highly responsive to climatic factors in addition to human activities. Among the most important factors impacting vegetation are precipitation and land surface temperature. Extreme temperatures and/or low precipitation might cause declining vegetation vigor and crop failures. A lack of rainfall could lead to surface moisture stress, making it difficult for plants to access the water they need to survive. Similarly, higher temperatures could generate thermal pressure for vegetation's photosynthesis and growth. Therefore, these

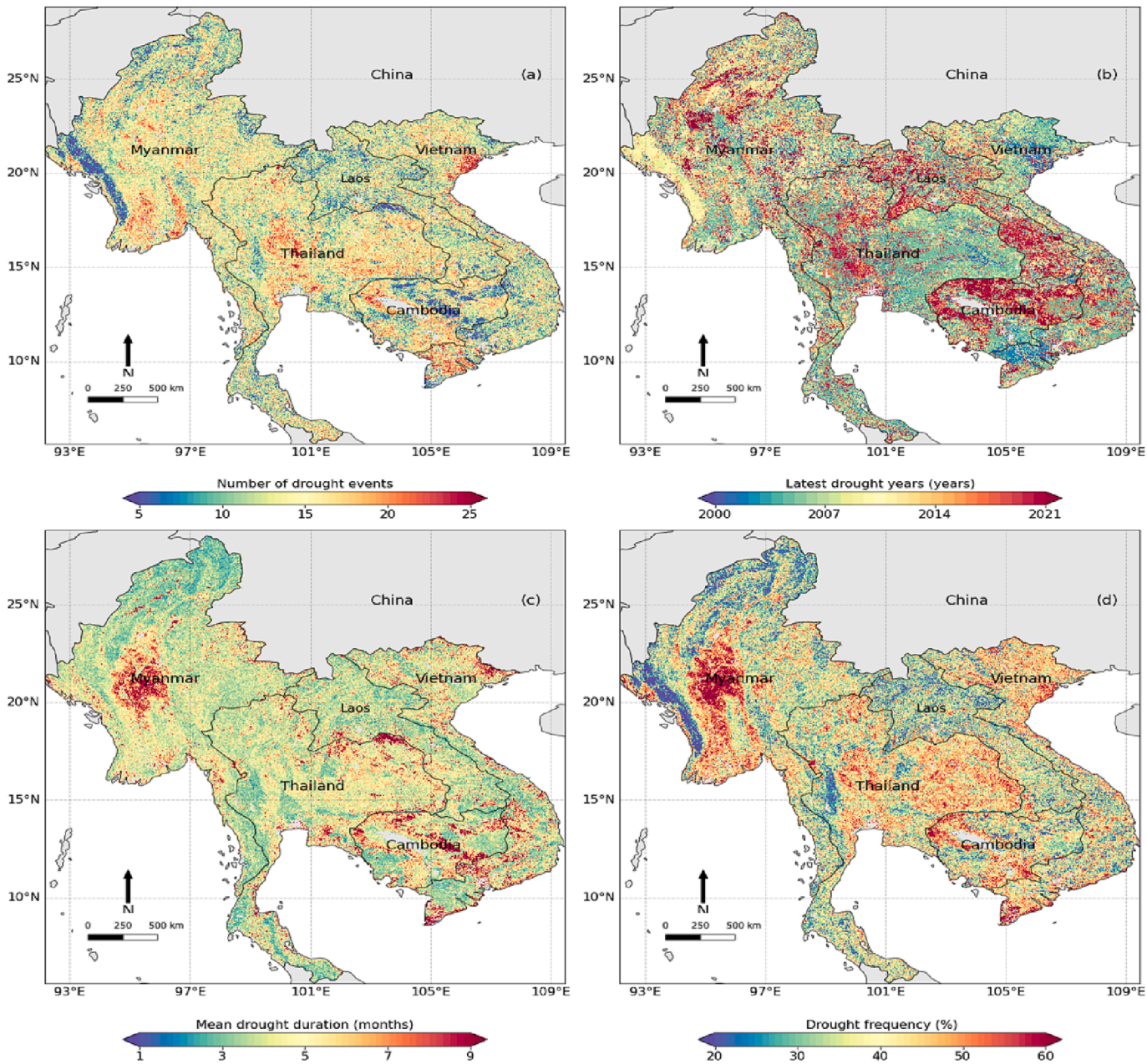


**Fig. 5.** Spatiotemporal characteristics of long-term drought conditions (a) longest vegetation stress, (b) the latest years of drought vegetation stress, (c) average vegetation stress duration, and (d) vegetation drought frequency over the MSEA region from 2000 to 2021.

variables can be used for evaluating the sensitivity of the VCI for drought monitoring.

The monthly R values between the VCI and temperature were performed across different land cover types (cropland, forestland, and shrubland) over the selected study period. Overall, the VCI and LST had a negative association in all vegetative areas (Fig. 3), but their relationships are characterized by the seasonal variations. The negative correlation revealed that increased temperature (drier weather) declined the VCI (increased vegetation stress). Obviously, higher absolute R values were mostly observed during the dry season, especially from January to March, while the wet season witnessed lower R values.

Obviously, this pattern is expected because the lack of water can limit plant growth and reduce vegetation cover during the dry season. In this context, temperature may have a greater influence on vegetation condition as it can affect plant water use efficiency and the rate of photosynthesis (Son et al., 2012). Hence, the correlation between the two datasets is stronger during this season due to higher sensitivity of vegetation to temperature under water limited conditions. By contrast, the rainy season typically provides plants with more moisture, resulting in increased growth and coverage that may reduce the impact of temperature on vegetation. As a result, the correlation in this case may be less pronounced compared to the dry season.

Considering the land cover types, the temporal pattern of R values was found to slightly vary across land cover classes, and cropland has the highest absolute R values (Fig. 3). Different land cover types can influence the correlation between the VCI and temperature in various ways. For example, forest generally have a higher transpiration rate than grasslands or croplands, making them less susceptible to temperature changes compared to other land cover classes (Wickham et al., 2012). By contrast, croplands are usually managed intensively to maximize productivity, which means that they are likely more sensitive to temperature changes than other land cover types (Marshall et al., 2004).

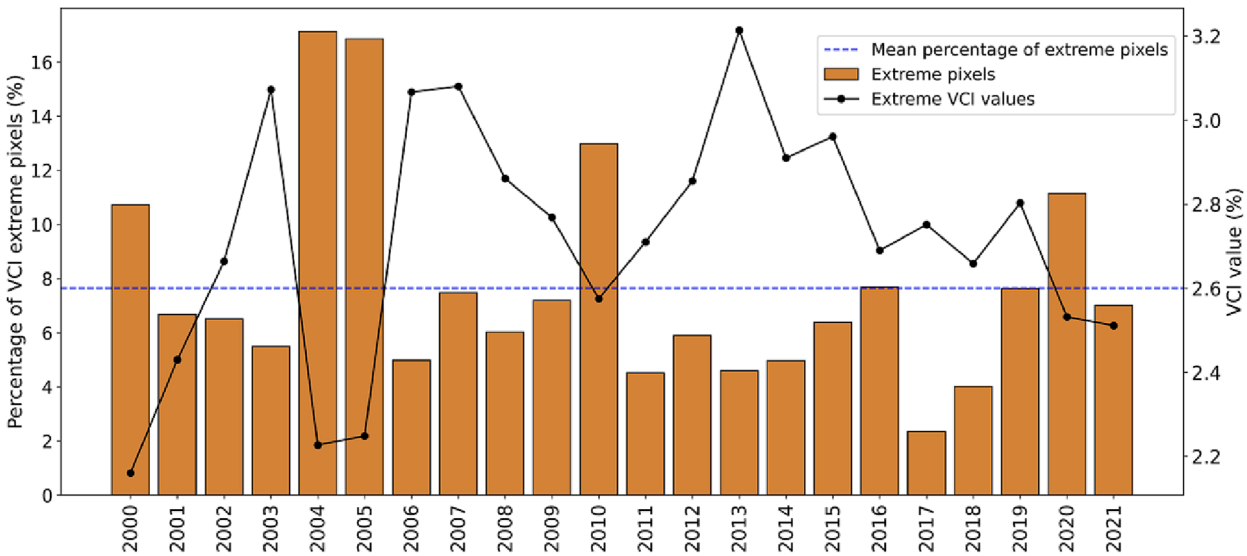


**Fig. 6.** The bar plot indicates annual percentage of extreme drought pixels over the MSEA from 2000 to 2021 whereas the line graph represents average extreme VCI severity. The dashed blue line indicates the average percentage of extreme pixels over the same period.

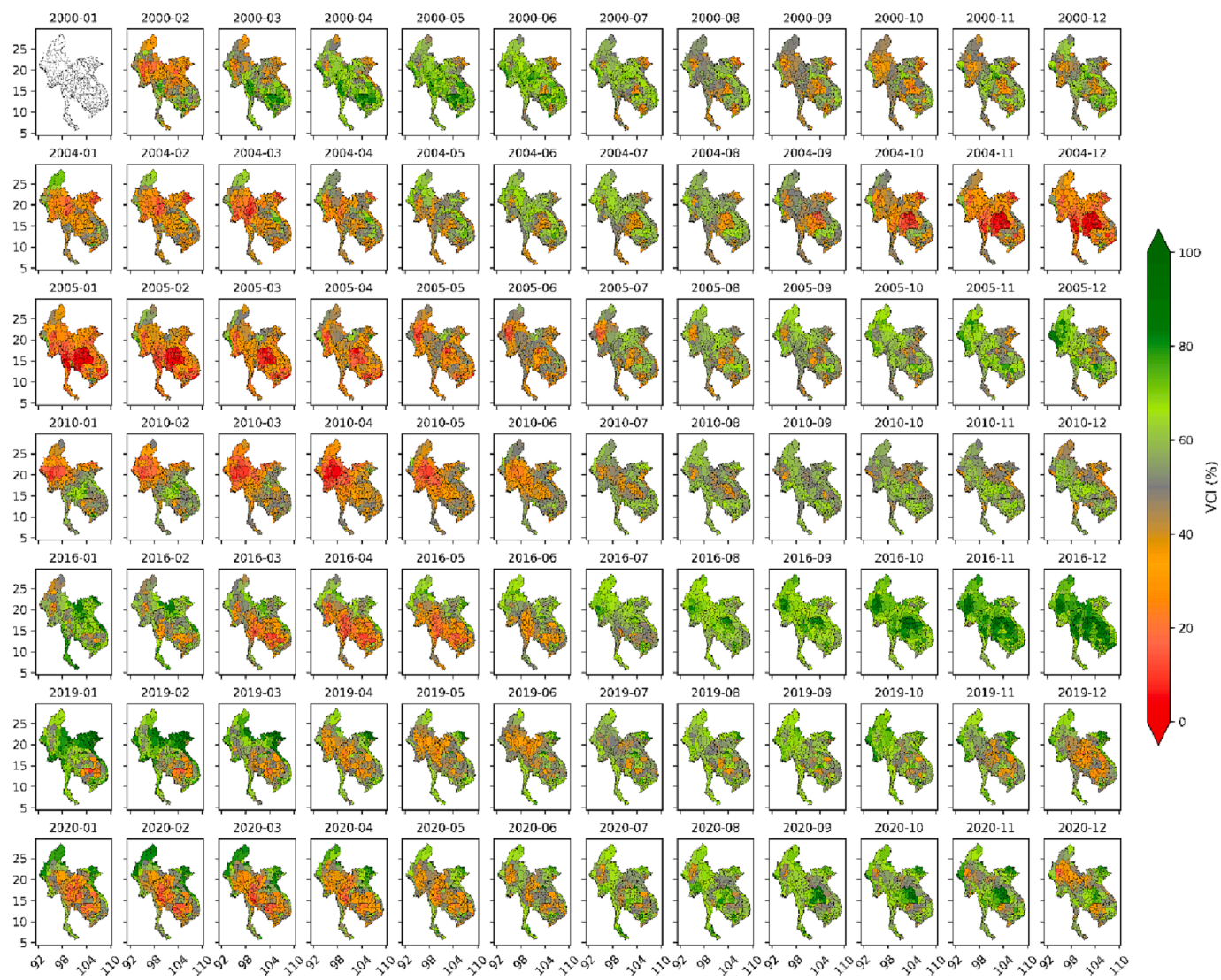


**Fig. 7.** Spatiotemporal variations of severe drought years over the MSEA. The VCI value was averaged by district/provincial administrative units. No data for January 2000.

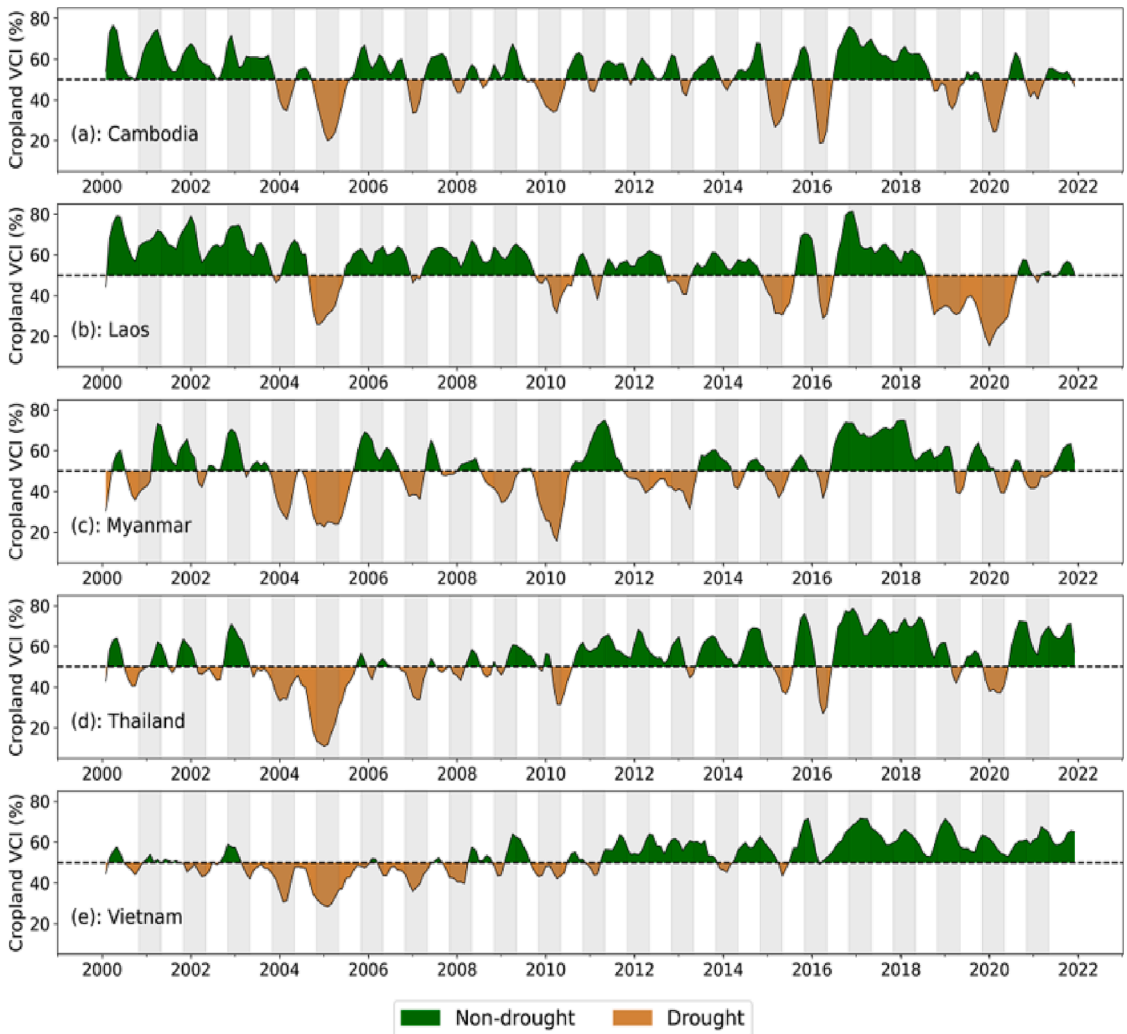


**Fig. 8.** Temporal variations of cropland VCI from 2000 to 2021 in Cambodia (a), Laos (b), Myanmar (c), Thailand (d), and Vietnam (e). Gray denotes the dry seasons.

The VCI results were also compared to the precipitation anomalies across vegetative types. The comparison revealed a close and consistent agreement between the VCI and precipitation over the selected time period (Fig. 4). Despite some discrepancies between the land cover classes, the closest agreement was observed in cropland areas, where the decline in VCI values was reflected in years with precipitation deficits (e.g., 2005, 2010, 2016, and 2019). This demonstrated that the VCI can reliably use for detecting crop stress and/or agricultural drought. In comparison, the VCI variability also followed precipitation deficits in forest and shrubland areas, but this trend was not as strong as in cropland areas. This suggests that the croplands are more responsive to rainfall than the other vegetative surfaces. These differences are most likely due to the sensitivity of forest and shrubland to droughts. Recent research has revealed that, compared to cropland and grassland, forest and shrubland areas are more resistant to drought conditions (Xu et al., 2018). Overall, the VCI-based drought demonstrated a reliable indicator for monitoring drought condition in the MSEA region.

### 4.2. Dynamics of drought characteristics in the MSEA region

#### 4.2.1. Spatiotemporal dynamics

Understanding the space–time drought characteristics is critical for risk mitigation management related to water resources and agricultural production. Fig. 5 presents the variability of four drought characteristics during the 2000–2021 period based on the VCI values. Prolonged drought events spatially varied across the region, with up to 25 events observed in southern Myanmar, Central Thailand, and the Red River delta (Fig. 5a). This result indicates typically longer periods of drought in these areas, which was consistent with in-situ drought reports. For example, the most recent drought recorded by the International Disaster Database in the lower Vietnamese Mekong provinces lasted nearly 8 months (Ha et al., 2022), whereas Thailand suffered from more than 15 months of drought.

On average, the MSEA region suffered from 12 to 15 drought events over the selected study period. Thailand had the highest number of prolonged droughts, with 14.5 events, followed by Vietnam (~12 events). Majority of the severe drought spells occurred in 2005 and 2016 (e.g., in Thailand and Vietnam), covering nearly 20% of the MSEA region. In recent years, the Lower Mekong Delta has disproportionately affected by prolonged drought events as compared to other areas (Fig. 5b). For example, the result indicates that nearly 35% of Cambodia experienced the prolonged drought during the years 2020 and 2021, which was consistent with the severe decline of major Tonle Sap Lake's water extent (Lindsay et al., 2021).

Except for differences in the latest drought years, there are common features between the drought duration and frequency. The mean duration is identified to be higher in Central Myanmar and the Lower Mekong areas (Fig. 5c). Consequently, the drought frequency was also observed to be larger there than in other areas (Fig. 3d). Overall, nearly 30% of the MSEA region suffered from more than 5 months of drought, and Cambodia had the highest mean duration of drought with nearly 6 months. Vietnam ranked second with nearly 5.2 months, while Laos had

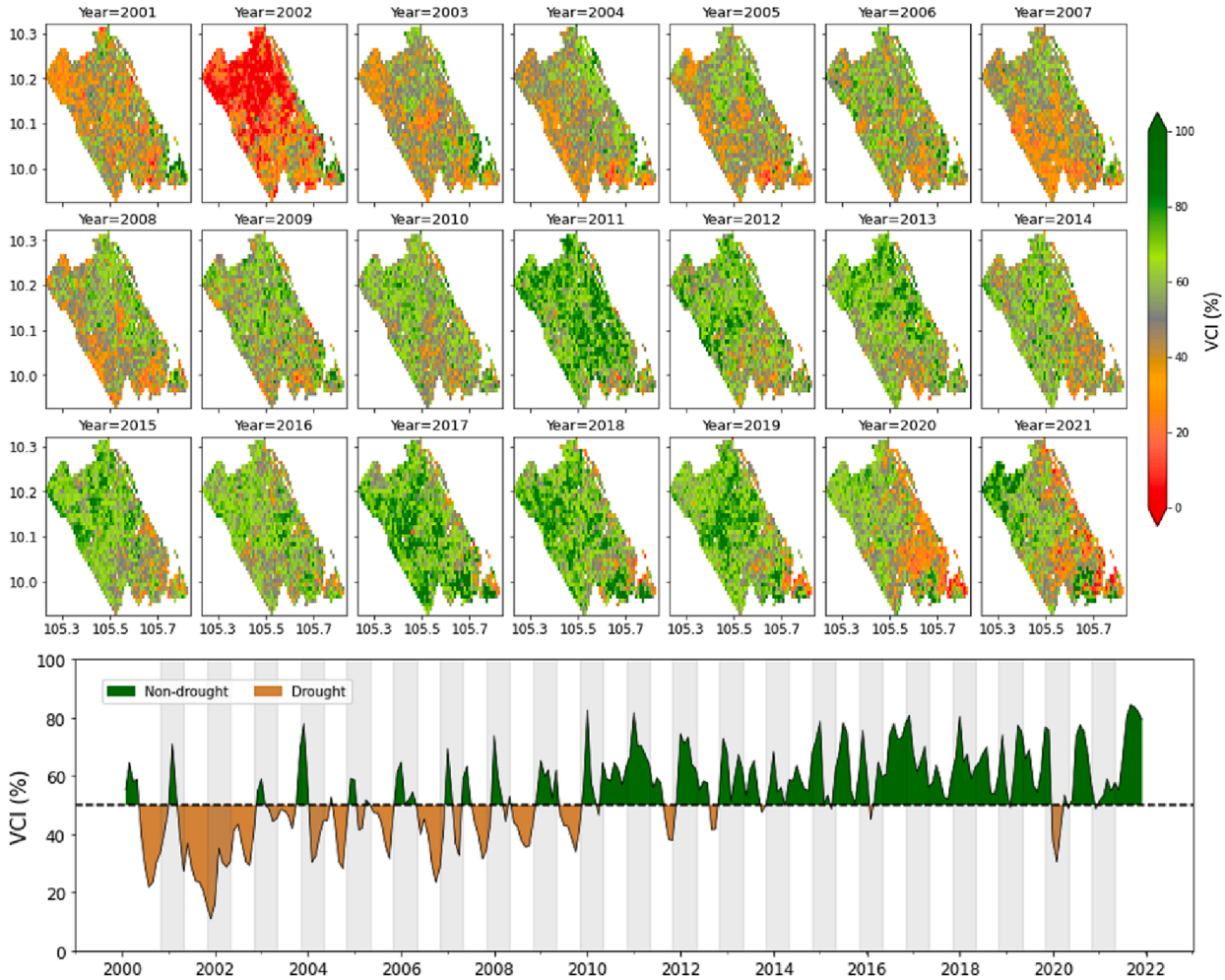


**Fig. 9.** Spatiotemporal distribution and evolution of agricultural drought conditions in Can Tho province, Vietnam during the dry seasons from 2000 to 2021. The line plot displays the temporal variations of crop stress. Gray bars in the line plot indicate the dry seasons.

the shortest duration with 4.3 months. In addition, the MSEA region was found to have a high drought frequency, particularly in cropland areas. On average, nearly 40% of droughts occurred in most countries, except for Laos, with 34%. Noticeably, the central region of Myanmar had the highest occurrence of drought (~60%), but with fewer prolonged drought events (Fig. 5a), implying shorter periods of drought in this area. In Vietnam, frequent drought conditions were mainly observed in Lower Mekong and Red River deltas (Fig. 5d), while Le et al. (2019) reported that drought frequency was largely found in Central Vietnam based on in-situ precipitation and temperature data from 1980 to 2014. These differences could be due to several factors such as selected thresholds, spatiotemporal resolutions, and sensitivity. For example, our study selected a threshold (VCI $\leq$ 50%) that indicates mild to extreme drought conditions, while they defined drought events from moderate to extreme conditions.

### 4.2.2. *Years of severe drought*

Fig. 6 illustrates the annual percentage of extreme pixels and VCI severity across the MSEA region. Overall, extreme pixels were variant across years, but the largest areas being impacted by drought were detected in 2000, 2004, 2005, 2010, 2016, 2019, and 2020. Noticeably, the years 2004 and 2005 had the highest percentage of extremely low VCI pixels (nearly 20%), followed by 2010 (~15%), whereas the most extreme VCI values were also observed during this period. Generally, larger extreme pixels are associated with lower extreme VCI values (Fig. 6).

The distribution of the severe drought years varied across space and time, with the majority of severe droughts detected during the dry season (Fig. 7). For instance, the longest drought event was observed in 2005 (~9 months), and the peak of this drought occurred between November 2004 and March 2005. Other severe drought years typically last from three to five months (e.g., 2016 and 2019). Spatially, severe drought conditions were found across the study area, but they were most commonly identified in Central Myanmar, Cambodia, and Thailand. Apparently, the entire MSEA region suffered from drought in the dry season of 2004–2005. In 2010, a severe drought occurred in the northern region (e.g., Myanmar). In comparison, the severe drought (2016) was mainly found in the southern region (e.g., Thailand and Cambodia). In addition, these countries have witnessed more severe drought than other locations in recent years.

The spatial evolution of drought years revealed that severe drought typically occurred from November/December to April/May, with the reoccurring cycle every 4–5 years. This period falls around the ripening of unirrigated rice fields (November-December) in Thailand, Myanmar, and Cambodia, whereas Vietnamese farmers begin the winter-spring rice cropping season. This information (drought onset and cessation) would be crucial for local authorities to navigate water resources and develop future drought mitigation plans. The results of this investigation revealed a close agreement with in-situ drought statistics and aligned with local drought studies. Vietnam, for example, suffered from the largest droughts in 2004–2005 (Tran et al., 2023) and 2005 and 2010 (Le et al., 2019). In the Lower Mekong Delta, severe drought years were

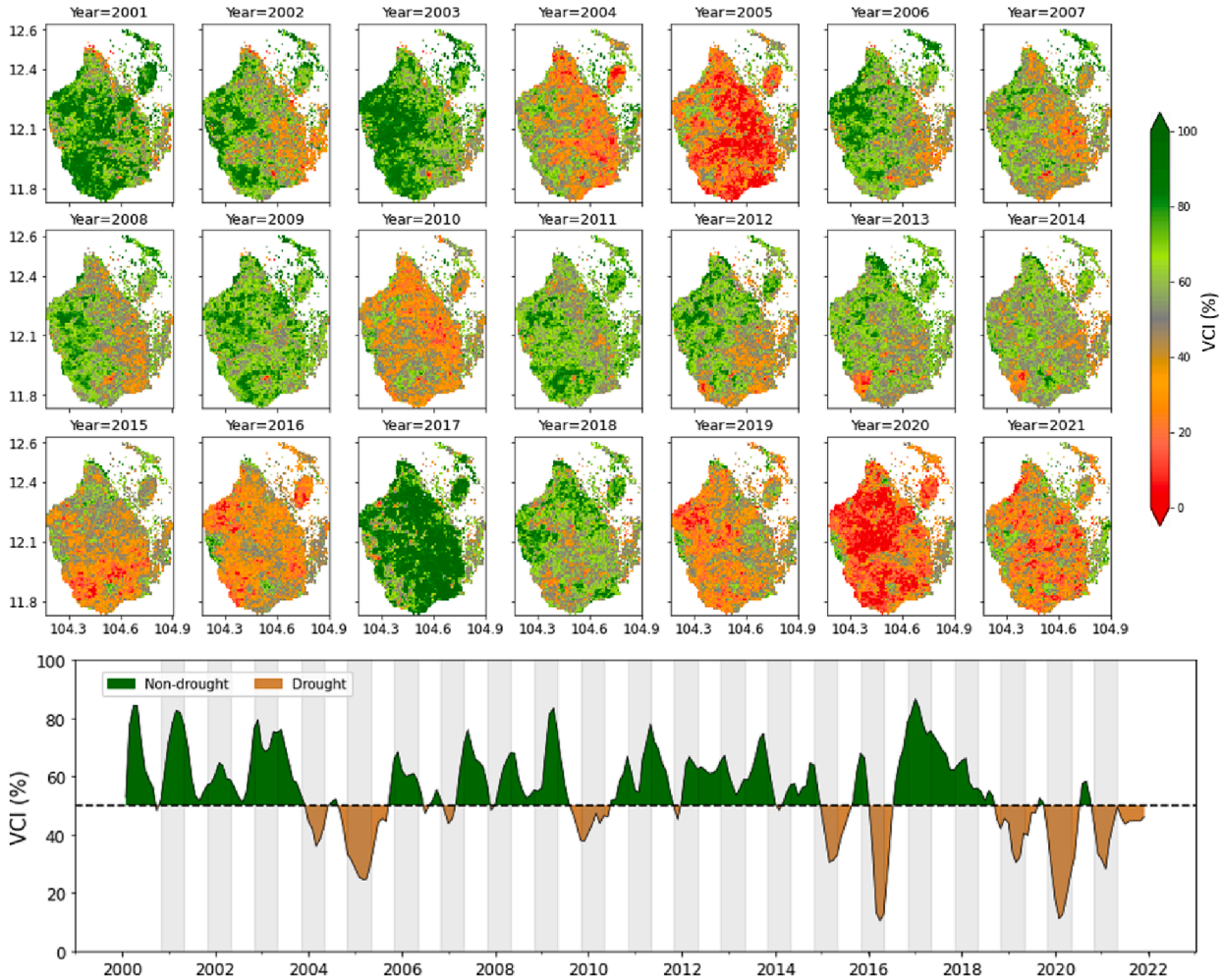


**Fig. 10.** Spatiotemporal evolution of agricultural drought conditions in Kompong Chnang province, Cambodia during the dry seasons from 2000 to 2021. The line plot displays temporal variations of crop stress. Gray bars in the line plot indicate the dry seasons.

reported in 2004–2005 (Adamson, 2005; Son et al., 2012), 2010 (Zhang et al., 2014), and 2015–2016 (Guo et al., 2017; Son and Thanh, 2022). A statistical analysis of in-situ drought events from the International Disaster Database revealed that the MSEA region suffered the largest drought events in 2005, 2010, 2015, 2016, and 2019 (Ha et al., 2022).

Although this approach demonstrated a promising result to identify severe drought years, there are some potential limitations. Firstly, the appropriate threshold value for drought detection using the VCI values may vary for different regions and data sources. Testing and validation of different threshold values are essential to ensure the accuracy of the results. Secondly, the spatial resolution of the VCI data can affect the results, and the VCI values may be influenced by insects and diseases or different land use practices, leading to different identification of drought years. However, it is expected that these factors are likely localized and may not represent large-area. For example, a pest outbreak in small areas of Thailand may cause a decline in the VCI values in that particular area but may not represent the overall drought condition over the entire MSEA region. Last but not the least, other factors may also influence severe drought years such as precipitation deficit, high temperature, and human activities. It is observed that nearly 85% of agricultural area in the MSEA remained rainfed-based practices, which suggest that the impact of irrigation is negligible. Despite its limitations, the VCI provided early signal and rich information on vegetation changes and drought conditions whereas the proposed approach can be expanded for other regions with similar climate and ecosystem characteristics to determine severe drought years.

#### 4.2.3. *Drought impacts on cropland vegetation*

The effects of drought on cropland vegetation can provide helpful insights on how crops respond to drought conditions across the environment over time. Fig. 8 shows the VCI-based drought evolution averaged by the country-wide cropland from 2000 to 2021. Overall, the patterns of drought dynamics were generally consistent across the countries, but there were great variations in recent years. For example, Laos and Cambodia suffered from the worst drought in 2020, whereas other countries showed little sign of drought conditions. Most countries had the lowest cropland VCI values (severe drought conditions) in 2005 (e.g., Thailand, Cambodia, and Vietnam), but Myanmar had lower cropland VCI values in 2010. Noticeably, Vietnam's cropland has suffered least from the drought over the last ten years (e.g., VCI $\geq$ 50), whereas the drought conditions had severe impacts in Thailand and Myanmar during the same period, as can be seen in Fig. 8.

To better understand the drought impacts in crop-growing regions, we further analyzed the spatiotemporal evolution of the droughts during the dry seasons in four specific areas where cropland is dominant. In highly irrigated cropland environments, the Vinh Phuc and Can Tho provinces of Vietnam suffered the least from drought conditions among the four examined areas. For instance, the worst drought event in Can Tho province was observed in the dry season 2002, whereas the remaining dry seasons usually experienced mild to moderate drought conditions (Fig. 9). As can be seen from the line plot in Fig. 9, croplands from 2000 to 2010 suffered from frequent droughts, and the latest droughts in this area were observed in 2020 and 2021. Although the

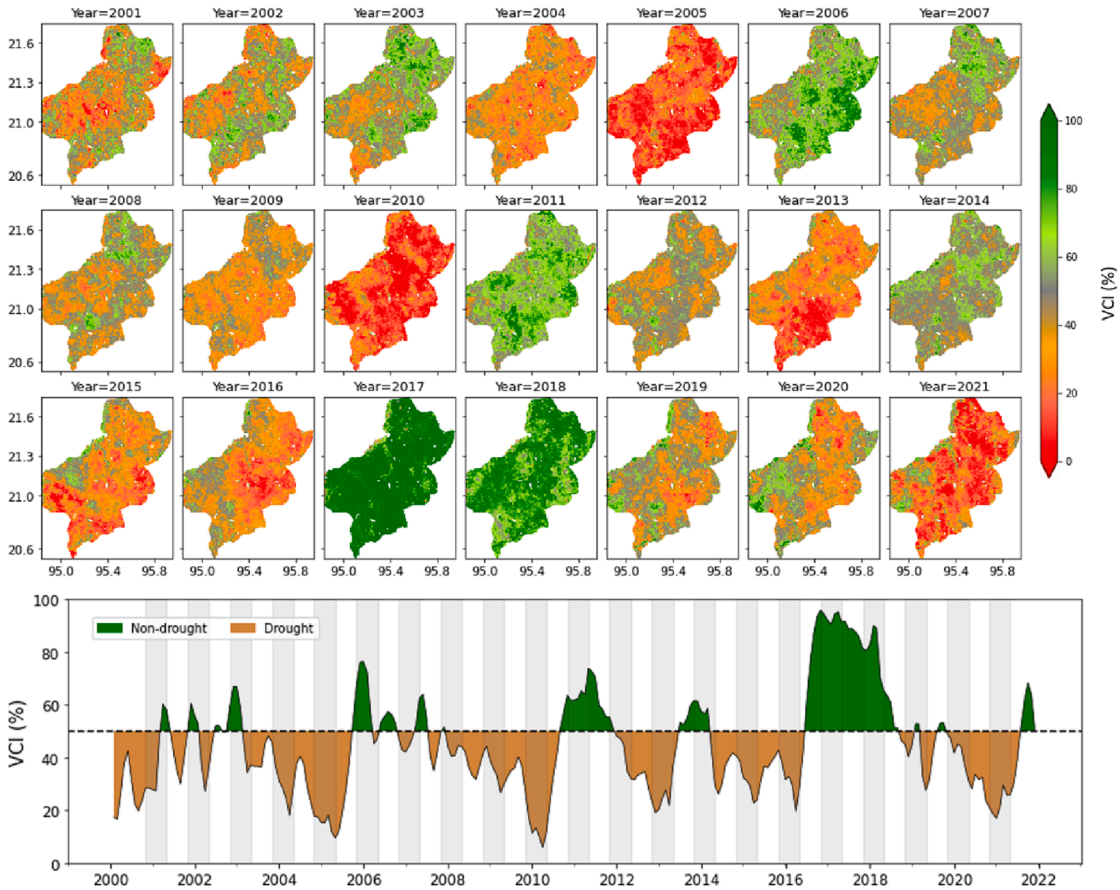


**Fig. 11.** Maps of spatiotemporal evolution of agricultural drought conditions in Myingan, Myanmar during the dry seasons from 2000 to 2021. The line plot displays temporal variations of crop stress. Gray bars in the line plot indicate the dry seasons.

VCI-based drought results showed moderate drought conditions, these recent droughts have been reported to cause significant damage to water supplies and livelihoods in the Lower Vietnamese Mekong Delta. A recent survey conducted in the coastal province of Soc Trang revealed the devastating impacts of drought stress on local farmers (Tran et al., 2021). Specifically, the survey found that the farmers' livelihoods and health are highly vulnerable to drought effects, but local food supplies remained sufficient. In 2015–2016 drought conditions were recorded in the Lower Vietnamese area, but the VCI results from the Fig. 9 showed that crop health remained good conditions, and this is likely due to the dense network of irrigation system in the region.

In comparison, the Kompong Chnang province of Cambodia has been frequently affected by severe drought conditions (Fig. 10). Despite its location downstream of the Tonle Sap Lake, the province has been hit hard by recent droughts in 2019 and 2020, which have caused significant damage to cropland areas. This is particularly evident in the dry period, when single-crop rainfed-based rice is commonly grown. Nearly 40% of the dry seasons in the province were observed with severe drought conditions (Fig. 10). The line graph in Fig. 10 depicts that the recent drought conditions have increased not only in frequency but also in magnitude. This information suggests that the recent droughts have become more severe and longer-lasting, which likely had great impacts on agricultural production and communities. Ha et al. (2022) revealed that Cambodia ranks second across the MSEA countries with nearly 9 million farmers affected by drought, whereas Son and Thanh (2022) estimated that more than 60 rice-growing Cambodian districts were largely affected in recent drought years.

In the central dry region of Myanmar, where rainfed legume and oilseed crops are the primary source of income for farmers (Herridge et al., 2019), but this area is increasingly prone to severe droughts, particularly during the dry seasons. For instance, croplands in Myingan were affected by severe drought conditions in most dry seasons (Fig. 11), which were worse compared to the other areas (e.g., Can Tho, Vietnam and Kompong Chnang, Cambodia). In a temporal sense, the croplands were most affected in 2005 and 2010, as shown in a line plot from Fig. 11. Interestingly, the greenest vegetation was observed in 2017 and 2018, which is a clear indication of favorable climatic conditions during these dry seasons. Although Myanmar frequently suffers from drought hazards, there has been little research in the recent decades. In fact, there have been no local and national drought studies using remote sensing time-series in Myanmar (Ha et al., 2022). Given the benefits of high spatiotemporal resolution satellite observations as well as vast agricultural landscape, there is a need to implement regular drought monitoring to strengthen the drought risk mitigation and support agricultural planning in this area.

### 4.3. Trend of drought conditions

Trend analyses were performed on the VCI time-series from 2000 to 2021. Fig. 12 displays the results of the per-pixel trend detected during both the dry and rainy growing seasons over the MSEA region. Green and red colors indicate decreasing and increasing drought conditions (or greening and browning vegetative trends), respectively, while gray colors represent non-significant trends or non-vegetative areas. Overall, decreasing drought conditions (increasing vegetation) predominate in northern Vietnam and eastern Thailand, whereas rising drought conditions (browning vegetation) are apparent in Cambodia and southern Laos. Regionally, this study found that nearly 15% of the vegetative areas suffered from increasing drought conditions, while the rest remained stable or resistant to drought hazards, with roughly 30% of the

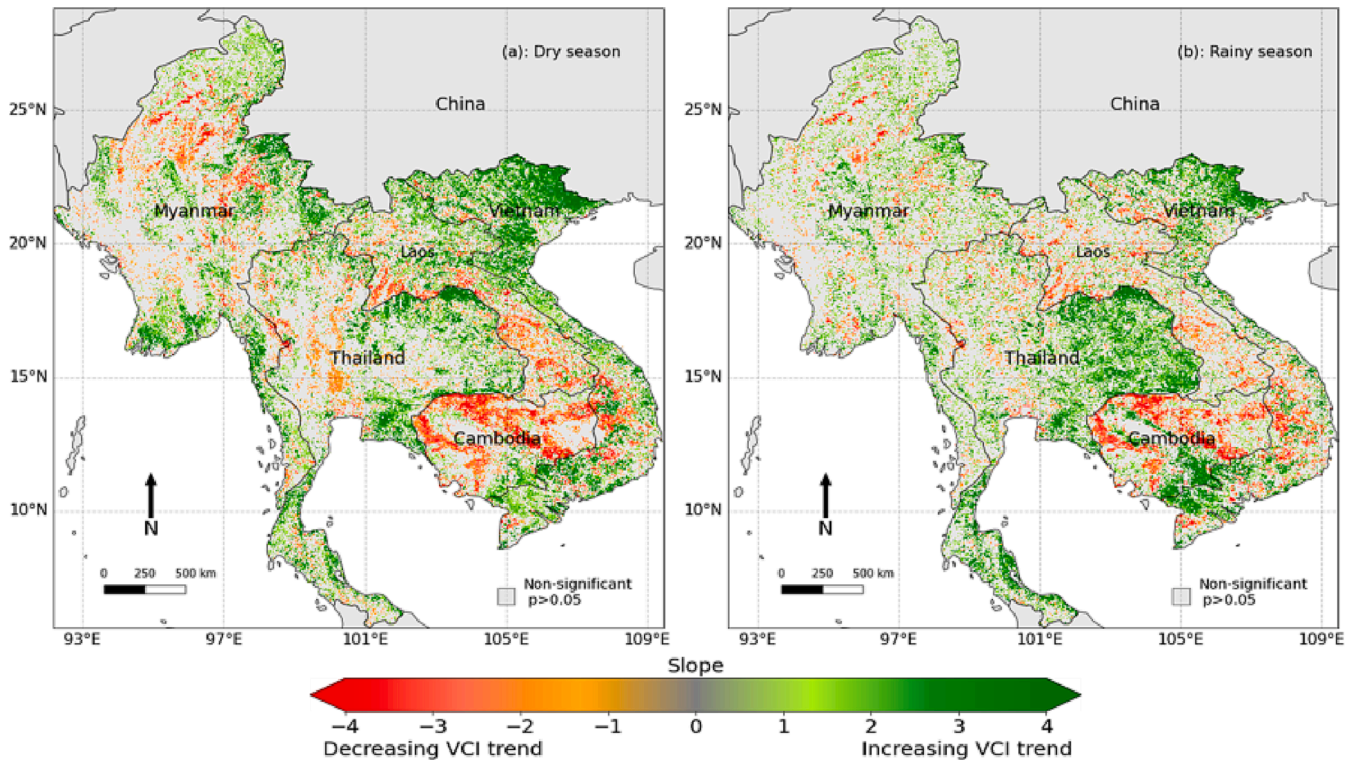


**Fig. 12.** Spatial variations of VCI sloping trend during the dry growing season (a) and rainy growing season (b) from 2000 to 2021 (unit: VCI [%] $yr^{-1}$). The increase of VCI values indicate the wetting trend, whereas the decline of VCI values represent the drying trend. The gray area indicates non-significant pixels (p-value > 0.05) or unvegetated areas/no data.

vegetation growing over the study period. These findings suggest that while some vegetative areas are more vulnerable to drought conditions, there are also areas and plants that are more resilient.

In the dry growing season, most of the forest or shrubland was found to indicate a decreasing trend of drought (an increase in green forest), whereas cropland shows either no trend or a slight change (Fig. 12a). In contrast, the trend analysis revealed that croplands experienced a decline in droughts (increase in greenness) during the rainy season in eastern Thailand and the lower Mekong delta. In Laos and Myanmar, vegetation greenness has remained relatively stable over the past 21 years (Fig. 12b). Moreover, the detected trend in northern Vietnam decreased from the dry to the rainy growing season.

Climate change and cropping practices could explain differences in the spatial variations of drought trends (vegetative stress). The increase of annual VCI is significant over northern Vietnam (VCI trend exceeds 4 $yr^{-1}$) where forests and shrubland are dominant. Over the past decade forest restoration programs from the Vietnamese government have increased forest cover in addition to the rapid expansion of farm-based forest plantations (de Jong, 2010). In Cambodia, a large decline of the VCI (e.g., rate $\leq$ -3 $yr^{-1}$) was prominent in the surrounding areas of the Tonle Sap Lake, where rainfed cropping systems are commonly practiced. Furthermore, Chen et al. (2021) analyzed the multi-decadal variability of Tonle Sap Lake, and they revealed that the lake's water extent has declined because of increasing climatic crises (e.g., precipitation deficits) and human activities (e.g., hydropower operations). In eastern Thailand, the rainfed rice crop is primarily grown in the rainy season, whereas flooding events usually occur during this time in northern Vietnam. These could be the possibilities of the increasing (decreasing) VCI drought trends in Thailand (Vietnam), respectively.

## 5. Conclusion and outlook

Drought has been and continues to have widespread impacts on agricultural production and the ecosystem. Understanding the dynamics of spatiotemporal drought variability plays a critical role in water resource management and risk mitigation for agricultural development and ecosystem protection. This study presented the first detailed analysis of spatiotemporal agricultural drought characteristics and trends over the MSEA region from 2000 to 2021 using the MODIS-based vegetation time-series data. A series of drought characteristics were investigated (e.g., duration, frequency, severe events, and the latest drought years) using the monthly VCI. Based on the annual extreme pixels, severe drought years were identified across the region. Lastly, the trend of drought was calculated based on the VCI time-series using the MK trend test in association with the Sen's slope for the dry and rainy growing seasons. The main results can be summarized the following:

- The patterns of drought characteristics vary in space and time over the MSEA region. Larger drought frequency and duration were found in central region of Myanmar and the Lower Mekong Delta. For example, Central Myanmar had the highest drought occurrence (~60%), whereas Thailand and Vietnam suffered from nearly 15 prolonged drought events over the past two decades.

- During the investigated period, the years 2000, 2004, 2005, 2010, 2016, 2019, and 2020 were found to be impacted by the most extreme drought conditions.

- A wetting trend was detected in Northern Vietnam during the dry season, whereas this trend is more dominant in eastern Thailand during the rainy season. The increase of drying conditions is significant over Cambodian cropland areas.

- Croplands were sensitive to drought conditions. In detail, croplands in Vietnam were observed to be least affected by drought conditions over the last ten years, whereas rainfed croplands in Cambodia and Myanmar suffered from severe droughts.

- A close agreement between the VCI-based drought and climatic factors was observed across time-series. The highest correlation coefficients between temperature and the VCI are observed during the dry

season.

The findings of this investigation could be of great value to regional and local authorities dealing with drought adaptation and mitigation strategies. For example, the drying trend in Cambodia and the higher drought frequency in Central Myanmar as well as the Lower Mekong Delta could be of relevance to decision-makers. The results of this study also demonstrated the advantages of the reconstructed MODIS-based vegetation time-series for continuously regional drought characterization. Given the fragmented cropland areas and increase in localized droughts in the MSEA region, details of space–time drought information are required for local agricultural planning. In the future, the potential of harmonized Landsat and Sentinel-2 observations will be explored with respect to drought monitoring and impact assessment, whereas driving factors of vegetation drought changes will be investigated.

## CRediT authorship contribution statement

**Tuyen V. Ha:** Data curation, Methodology, Formal analysis, Visualization, Writing – original draft, Writing – review & editing. **Soner Uereyen:** Writing – review & editing. **Claudia Kuenzer:** Supervision, Conceptualization.

## Declaration of Competing Interest

The authors declare that they have no known competing financial interests or personal relationships that could have appeared to influence the work reported in this paper.

## Data availability

Data will be made available on request.

## Acknowledgements

This work was supported by the German Ministry of Education and Research (No. 01LZ2002A) and the DAAD Research Grant Program in Germany (No. 91794761).

## References

Adamson, P., 2005. Drought study: analysis, forecasting, planning and management. Mekong River Commission, Vientiane, Laos.
Amnuaylojaroen, T., Chanvichit, P., 2019. Projection of near-future climate change and agricultural drought in Mainland Southeast Asia under RCP8. 5. Clim. Change 155, 175–193.
Bajgiran, P.R., Darvishsefat, A.A., Khalili, A., Makhdoum, M.F., 2008. Using AVHRR-based vegetation indices for drought monitoring in the Northwest of Iran. J. Arid Environ. 72, 1086–1096.
Chen, J., Jönsson, P., Tamura, M., Gu, Z., Matsushita, B., Eklundh, L., 2004. A simple method for reconstructing a high-quality NDVI time-series data set based on the Savitzky-Golay filter. Remote Sens. Environ. 91, 332–344.
Chen, A., Liu, J., Kummu, M., Varis, O., Tang, Q., Mao, G., Wang, J., Chen, D., 2021. Multidecadal variability of the Tonle Sap Lake flood pulse regime. Hydrol. Processes 35, e14327.
Dandridge, C., Lakshmi, V., Bolten, J., Srinivasan, R., 2019. Evaluation of satellite-based rainfall estimates in the lower mekong river basin (southeast asia). Remote Sens. 11, 2709.
de Jong, W., 2010. Forest rehabilitation and its implication for forest transition theory. Biotropica 42, 3–9.
Didan, K., 2021. MODIS/Terra Vegetation Indices 16-Day L3 Global 500m SIN Grid V061. NASA EOSDIS Land Processes DAAC.
Didan, K., Munoz, A.B., Solano, R., Huete, A., 2015. MODIS vegetation index user's guide (MOD13 series). University of Arizona, Vegetation Index and Phenology Lab.
Ding, Y., Hayes, M.J., Widhalm, M., 2011. Measuring economic impacts of drought: a review and discussion. Disaster Prevention and Management: An. Int. J.
Dracup, J.A., Lee, K.S., Paulson Jr, E.G., 1980. On the definition of droughts. Water Resour. Res. 16, 297–302.
Du, L., Tian, Q., Yu, T., Meng, Q., Jancso, T., Udvardy, P., Huang, Y., 2013. A comprehensive drought monitoring method integrating MODIS and TRMM data. Int. J. Appl. Earth Obs. Geoinf. 23, 245–253.
Dutta, D., Kundu, A., Patel, N., Saha, S., Siddiqui, A., 2015. Assessment of agricultural drought in Rajasthan (India) using remote sensing derived Vegetation Condition Index (VCI) and Standardized Precipitation Index (SPI). Egypt. J. Remote Sens. Space Sci. 18, 53–63.
ESA, 2017. European Space Agency Land Cover CCI Product User Guide.
Fan, C., Myint, S.W., Rey, S.J., Li, W., 2017. Time series evaluation of landscape dynamics using annual Landsat imagery and spatial statistical modeling: Evidence from the Phoenix metropolitan region. Int. J. Appl. Earth Obs. Geoinf. 58, 12–25.
Funk, C., Peterson, P., Landsfeld, M., Pedreros, D., Verdin, J., Shukla, S., Husak, G., Rowland, J., Harrison, L., Hoell, A., 2015. The climate hazards infrared precipitation with stations—a new environmental record for monitoring extremes. Scientific data 2, 1–21.
Gebrehiwot, T., Van der Veen, A., Maathuis, B., 2011. Spatial and temporal assessment of drought in the Northern highlands of Ethiopia. Int. J. Appl. Earth Obs. Geoinf. 13, 309–321.
Guo, H., Bao, A., Liu, T., Ndayisaba, F., He, D., Kurban, A., De Maeyer, P., 2017. Meteorological drought analysis in the Lower Mekong Basin using satellite-based long-term CHIRPS product. Sustainability 9, 901.
Guo, H., Bao, A., Liu, T., Ndayisaba, F., Jiang, L., Kurban, A., De Maeyer, P., 2018. Spatial and temporal characteristics of droughts in Central Asia during 1966–2015. Sci. Total Environ. 624, 1523–1538.
Ha, T.V., Huth, J., Bachofer, F., Kuenzer, C., 2022. A Review of Earth Observation-Based Drought Studies in Southeast Asia. Remote Sens. 14, 3763.
Herridge, D.F., Win, M.M., Nwe, K.M.M., Kyu, K.L., Win, S.S., Shwe, T., Min, Y.Y., Denton, M.D., Cornish, P.S., 2019. The cropping systems of the Central Dry Zone of Myanmar: Productivity constraints and possible solutions. Agricultural Systems 169, 31–40.
Huete, A.R., 1988. A soil-adjusted vegetation index (SAVI). Remote Sens. Environ. 25, 295–309.
Jiao, W., Wang, L., McCabe, M.F., 2021. Multi-sensor remote sensing for drought characterization: current status, opportunities and a roadmap for the future. Remote Sens. Environ. 256, 112313.
Kogan, F.N., 1990. Remote sensing of weather impacts on vegetation in non-homogeneous areas. Int. J. Remote Sens. 11, 1405–1419.
Kogan, F.N., 1995a. Application of vegetation index and brightness temperature for drought detection. Adv. Space Res. 15, 91–100.
Kogan, F.N., 1995b. Droughts of the late 1980s in the United States as derived from NOAA polar-orbiting satellite data. Bull. Am. Meteorol. Soc. 76, 655–668.
Kuenzer, C., Knauer, K., 2013. Remote sensing of rice crop areas. Int. J. Remote Sens. 34, 2101–2139.
Le, M.-H., Kim, H., Moon, H., Zhang, R., Lakshmi, V., Nguyen, L.-B., 2020. Assessment of drought conditions over Vietnam using standardized precipitation evapotranspiration index, MERRA-2 re-analysis, and dynamic land cover. J. Hydrol.: Regional Stud. 32, 100767.
Le, P.V., Phan-Van, T., Mai, K.V., Tran, D.Q., 2019. Space–time variability of drought over Vietnam. Int. J. Climatol. 39, 5437–5451.
Leinenkugel, P., Kuenzer, C., Dech, S., 2013. Comparison and enhancement of MODIS cloud mask products for Southeast Asia. Int. J. Remote Sens. 34, 2730–2748.
Li, Y., Lu, H., Entekhabi, D., Gianotti, D.J.S., Yang, K., Luo, C., Feldman, A.F., Wang, W., Jiang, R., 2022. Satellite-Based Assessment of Meteorological and Agricultural Drought in Mainland Southeast Asia. IEEE J. Sel. Top. Appl. Earth Observ. Remote Sens. 15, 6180–6189.
Li, B., Su, H., Chen, F., Wu, J., Qi, J., 2013. The changing characteristics of drought in China from 1982 to 2005. Nat. Hazards 68, 723–743.
Liang, L., Sun, Q., Luo, X., Wang, J., Zhang, L., Deng, M., Di, L., Liu, Z., 2017. Long-term spatial and temporal variations of vegetative drought based on vegetation condition index in China. Ecosphere 8, e01919.
Lindsay, J., Gaba, K., Harmon, L., Jarvis, S., 2021. Tonlé Sap Food Security & Agriculture III: Evaluating Changes in Ecosystem Vitality and Freshwater Health in the Tonlé Sap Basin using Remotely Sensed Data.
Lingfeng, L., Bo, Q., Weidong, G., Yiping, Z., Qinghai, S., Jiuyi, C., 2022. Phenological and physiological responses of the terrestrial ecosystem to the 2019 drought event in Southwest China: Insights from satellite measurements and the SSiB2 model. Int. J. Appl. Earth Obs. Geoinf. 111, 102832.
Liu, W., Kogan, F., 1996. Monitoring regional drought using the vegetation condition index. Int. J. Remote Sens. 17, 2761–2782.
Mao, D., Wang, Z., Luo, L., Ren, C., 2012. Integrating AVHRR and MODIS data to monitor NDVI changes and their relationships with climatic parameters in Northeast China. Int. J. Appl. Earth Obs. Geoinf. 18, 528–536.
Marshall, C.H., Pielke Sr, R.A., Steyaert, L.T., Willard, D.A., 2004. The impact of anthropogenic land-cover change on the Florida peninsula sea breezes and warm season sensible weather. Monthly Weather Rev. 132, 28–52.
McKee, T.B., Doesken, N.J., Kleist, J., 1993. The relationship of drought frequency and duration to time scales, Proceedings of the 8th Conference on Applied Climatology. Boston, MA, USA, pp. 179–183.
Mishra, A.K., Singh, V.P., 2010. A review of drought concepts. J. Hydrol. 391, 202–216.
Muthumanickam, D., Kannan, P., Kumaraperumal, R., Natarajan, S., Sivasamy, R., Poongodi, C., 2011. Drought assessment and monitoring through remote sensing and GIS in western tracts of Tamil Nadu. India. Int. J. Remote Sens. 32, 5157–5176.
Qian, X., Liang, L., Shen, Q., Sun, Q., Zhang, L., Liu, Z., Zhao, S., Qin, Z., 2016. Drought trends based on the VCI and its correlation with climate factors in the agricultural areas of China from 1982 to 2010. Environ. Monit. Assess. 188, 1–13.
Ruefenacht, B., 2016. Comparison of three Landsat TM compositing methods: a case study using modeled tree canopy cover. Photogramm. Eng. Remote Sens. 82, 199–211.
Sen, P.K., 1968. Estimates of the regression coefficient based on Kendall's tau. J. Am. Statist. Assoc. 63, 1379–1389.
Shahabfar, A., Ghulam, A., Eitzinger, J., 2012. Drought monitoring in Iran using the perpendicular drought indices. Int. J. Appl. Earth Obs. Geoinf. 18, 119–127.

Son, N.T., Chen, C., Chen, C., Chang, L., Minh, V.Q., 2012. Monitoring agricultural drought in the Lower Mekong Basin using MODIS NDVI and land surface temperature data. Int. J. Appl. Earth Obs. Geoinf. 18, 417–427.
Son, N.T., Thanh, B.X., 2022. Remotely sensed drought evaluation over rice cultivated areas in Cambodia during 2000 to 2019. Geocart. Internat. 37, 1237–1255.
Svoboda, M.D., Fuchs, B.A., 2016. Handbook of drought indicators and indices. World Meteorological Organization Geneva, Switzerland.
Tarpley, J., Schneider, S., Money, R., 1984. Global vegetation indices from the NOAA-7 meteorological satellite. J. Clim. Appl. Meteorol. 491–494.
Tran, T.V., Bruce, D., Huang, C.-Y., Tran, D.X., Myint, S.W., Nguyen, D.B., 2023. Decadal assessment of agricultural drought in the context of land use land cover change using MODIS multivariate spectral index time-series data. GIScience & Remote Sensing 60, 2163070.
Tran, D.D., Dang, M.M., Du Duong, B., Sea, W., Vo, T.T., 2021. Livelihood vulnerability and adaptability of coastal communities to extreme drought and salinity intrusion in the Vietnamese Mekong Delta. Int. J. Disaster Risk Reduction 57, 102183.
Unescap, 2019. Asia-Pacific Disaster Report 2019. United Nations Bangkok.
Unganai, L.S., Kogan, F.N., 1998. Drought monitoring and corn yield estimation in Southern Africa from AVHRR data. Remote Sens. Environ. 63, 219–232.
Venkatappa, M., Sasaki, N., Han, P., Abe, I., 2021. Impacts of droughts and floods on croplands and crop production in Southeast Asia–An application of Google Earth Engine. Sci. Total Environ. 795, 148829.
Vicente-Serrano, S.M., Beguería, S., López-Moreno, J.I., 2010. A multiscalar drought index sensitive to global warming: the standardized precipitation evapotranspiration index. J. Clim. 23, 1696–1718.
Wickham, J.D., Wade, T.G., Riitters, K.H., 2012. Comparison of cropland and forest surface temperatures across the conterminous United States. Agr. Forest Meteorol. 166, 137–143.
Wilhite, D.A., Glantz, M.H., 1985. Understanding: the drought phenomenon: the role of definitions. Water Int. 10, 111–120.
Winkler, K., Gessner, U., Hochschild, V., 2017. Identifying droughts affecting agriculture in Africa based on remote sensing time series between 2000–2016: rainfall anomalies and vegetation condition in the context of ENSO. Remote Sens. 9, 831.
Xie, F., Fan, H., 2021. Deriving drought indices from MODIS vegetation indices (NDVI/EVI) and Land Surface Temperature (LST): Is data reconstruction necessary? Int. J. Appl. Earth Obs. Geoinf. 101, 102352.
Xu, H.-J., Wang, X.-P., Zhao, C.-Y., Yang, X.-M., 2018. Diverse responses of vegetation growth to meteorological drought across climate zones and land biomes in northern China from 1981 to 2014. Agr. Forest Meteorol. 262, 1–13.
Yan, N., Wu, B., Boken, V.K., Chang, S., Yang, L., 2016. A drought monitoring operational system for China using satellite data: design and evaluation. Geomatics, Nat. Hazards Risk 7, 264–277.
Zhang, L., Chen, Z., Zhou, T., 2021. Human influence on the increasing drought risk over Southeast Asian monsoon region. Geophys. Res. Lett. 48, e2021GL093777.
Zhang, B., Zhang, L., Guo, H., Leinenkugel, P., Zhou, Y., Li, L., Shen, Q., 2014. Drought impact on vegetation productivity in the Lower Mekong Basin. Int. J. Remote Sens. 35, 2835–2856.